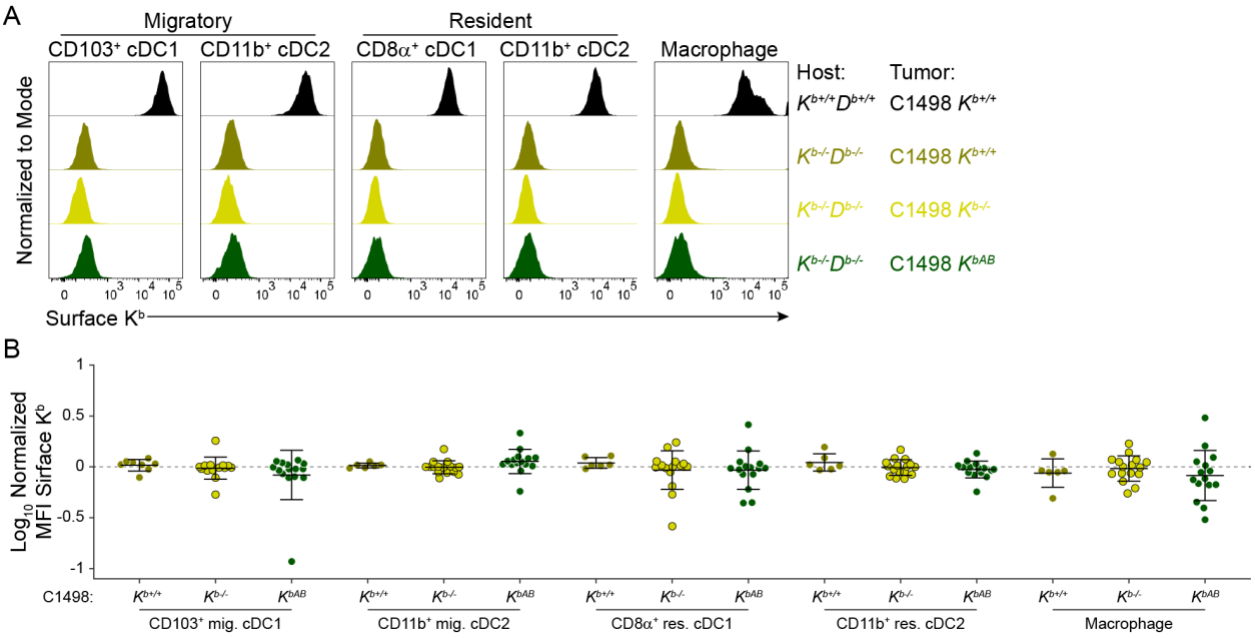

Supplemental Figure S1 (related to Figure 4): C1498-derived K^b molecules are not detected on the surface of tdLN APCs by flow cytometry. A and B) Surface staining for K^b on tdLN APCs from *K$^{b-/-}$D$^{b-/-}$* mice bearing C1498 *K$^{b+/+}$* (n = 6), *K$^{b-/-}$* (n = 16), and *K^{bAB}* (n = 15) tumors at day 6-10. Representative flow cytometry histograms (A) and data quantification (B) are shown. Data are pooled from four independent experiments and depicted as mean ± s.d. Statistical significance was determined by two-way ANOVA with post-hoc Tukey's HSD test.

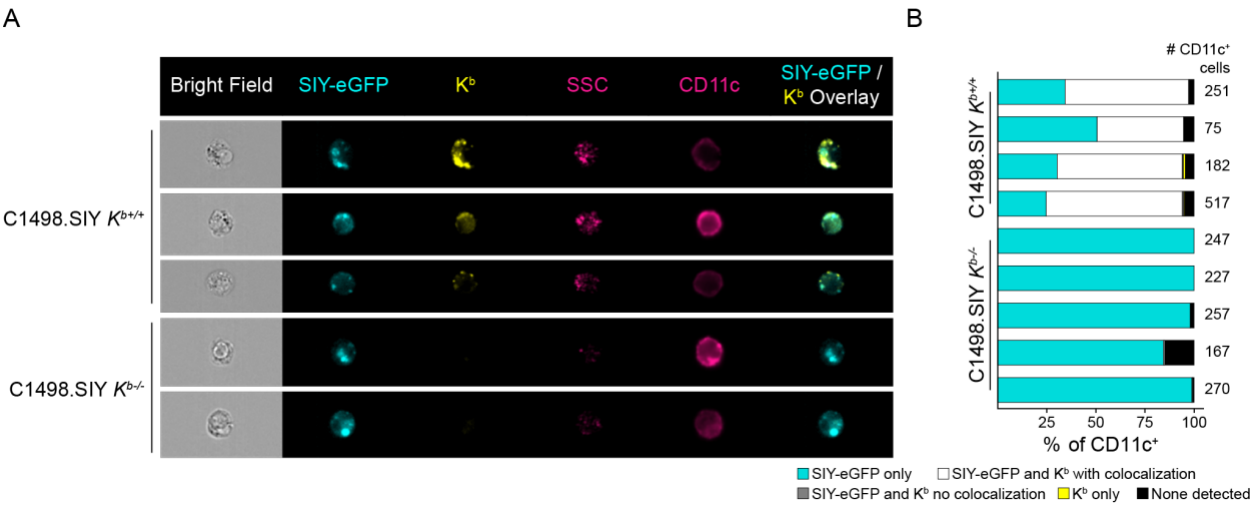

Supplemental Figure S2 (Related to Figure 4): Correlation between acquisition of tumor-derived K^b molecules and internalization of a fluorescent tumor antigen. CD11c$^+$ APCs isolated from 7-day C1498.SIY *K*$^{b+/+}$ or *K*$^{b-/-}$ tumors in *K*$^{b-/-}$*D*$^{b-/-}$ mice were analyzed by imaging flow cytometry. **A)** Representative images of CD11c$^+$ APCs showing internalization of model tumor antigen (SIY-eGFP) and acquisition of tumor-derived K^b molecules by intracellular antibody stain. **B)** Summary bar graph of the data. Each bar represents one mouse, and the number of CD11c$^+$ APCs imaged is indicated to the right. Three samples were excluded from the quantification because fewer than 50 CD11c$^+$ APCs were imaged in focus. Data shown are from one experiment, representative of two independent experiments.

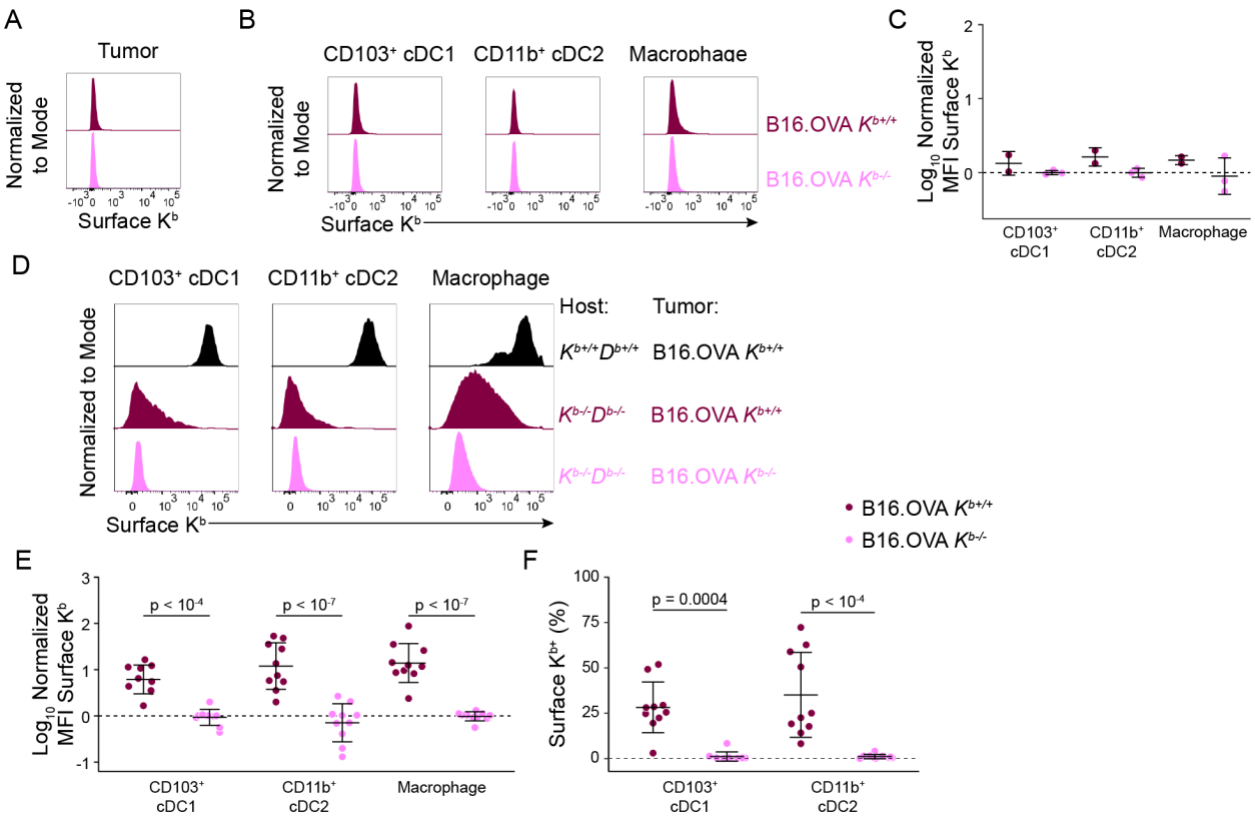

Supplemental Figure S3 (Related to Figure 4): Acquisition of B16.OVA-derived Kᵇ molecules by APC populations in the tumor. A-C) *Kᵇ⁻/⁻Dᵇ⁻/⁻* mice bearing B16.OVA *Kᵇ⁺/⁺* (n = 2) or *Kᵇ⁻/⁻* (n = 3) tumors, which were analyzed for cell surface Kᵇ expression at day 6-10. Surface staining for Kᵇ is shown for tumor cells (A) and tumor-resident APCs (B). Quantified data are in (C). Data shown are from one experiment, representative of two independent experiments. **D-F)** B16.OVA *Kᵇ⁺/⁺* and *Kᵇ⁻/⁻* cells were pre-treated with IFN-γ for 48 hr *in vitro* prior to inoculation into C57BL/6 or *Kᵇ⁻/⁻Dᵇ⁻/⁻* hosts (n = 10 for each tumor). Representative flow cytometry histograms of Kᵇ surface staining are shown on APCs (D). Data are quantified as mean fluorescence intensity (E) and percent Kᵇ⁺ (F). Data in (E) and (F) are pooled from three independent experiments, and all summary plots are depicted as mean ± s.d. Statistical significance was determined by two-way ANOVA with post-hoc Tukey's HSD.

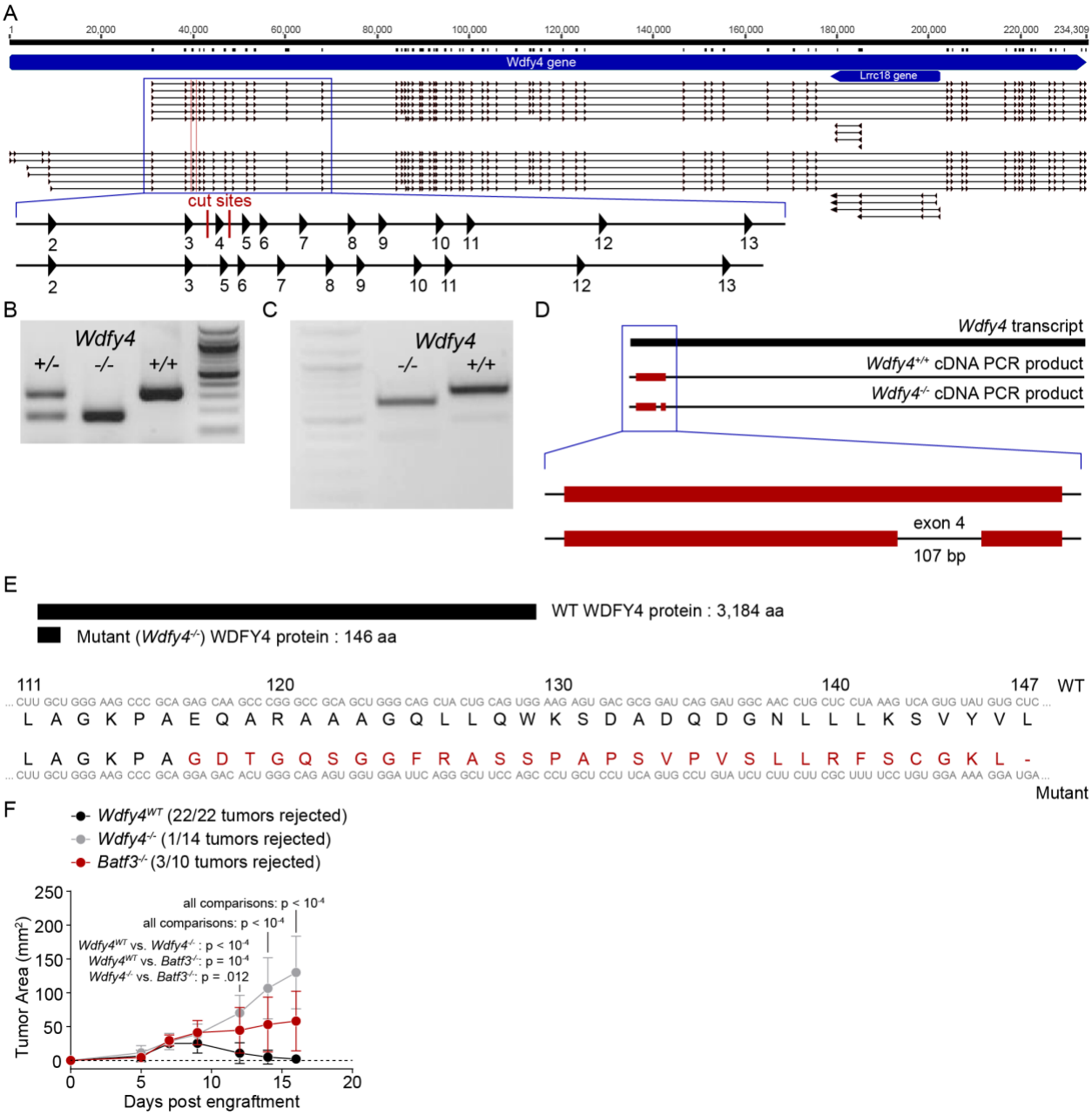

Supplemental Figure S4 (Related to Figure 6): Generation of *Wdfy4*$^{-/-}$ mice. A) Illustration of the *Wdfy4* gene depicting the exons in different splice variants, with gRNA target sites indicated flanking exon 4. **B)** PCR amplification of genomic DNA surrounding exon 4, with a 144 bp excision in the *Wdfy4*$^{-/-}$ allele. **C and D)** RT-PCR amplification of a segment of the *Wdfy4* transcript containing exon 4 from *Wdfy4*$^{+/+}$ and *Wdfy4*$^{-/-}$ splenocytes, with a 107 bp deletion in the *Wdfy4*$^{-/-}$

allele. Alignment of the amplified cDNA fragments are shown in red. **E)** Illustration showing the length of proteins encoded by *Wdfy4*$^{+/+}$ and *Wdfy4*$^{-/-}$ alleles (to scale), along with RNA (grey) and translated amino acid sequences (wild-type and consensus sequences shown in black and the mutated region depicted in red) in the region containing the frameshift mutation and stop codon. **F)** Growth curves of 1969 tumors in littermate *Wdfy4*^{WT} and *Wdfy4*$^{-/-}$ mice, as well as in *Batf3*$^{-/-}$ mice. Statistical significance was determined by two-way ANOVA with Sidak's post-hoc test for multiple comparisons. Data are depicted as mean ± s.d. and pooled from two independent experiments.

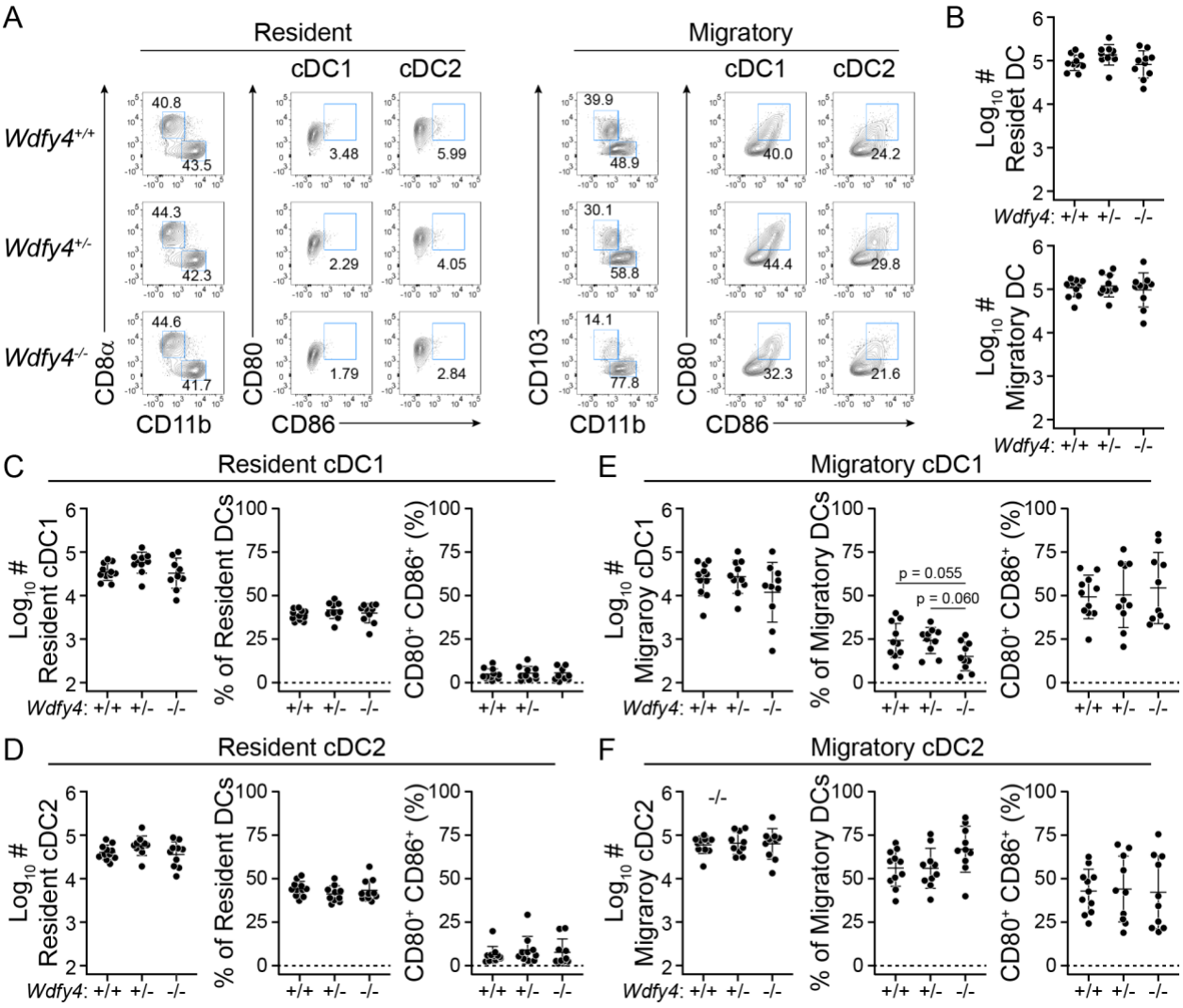

Supplemental Figure S5 (Related to Figure 6): Normal cDC development and costimulatory molecule expression in cutaneous LNs of *Wdfy4*$^{-/-}$ mice. A) Representative flow cytometry plots of cDC populations in pooled cLNs of *Wdfy4*$^{+/+}$, *Wdfy4*$^{+/-}$, and *Wdfy4*$^{-/-}$ mice. **B)** Resident and migratory cDC numbers in pooled cLNs of *Wdfy4*$^{+/+}$ (n = 11), *Wdfy4*$^{+/-}$ (n = 10), and *Wdfy4*$^{-/-}$ (n = 10) mice. **C-F)** Quantification of numbers, frequency, and CD80/CD86 expression data for resident CD8α^{+} cDC1 (C), resident CD11b^{+} cDC2 (D), migratory CD103^{+} cDC1 (E), and migratory CD11b^{+} cDC2 (F) in pooled cLNs. Statistical significance was determined by one-way ANOVA with post-hoc Tukey's HSD test. Data are pooled from three independent experiments.

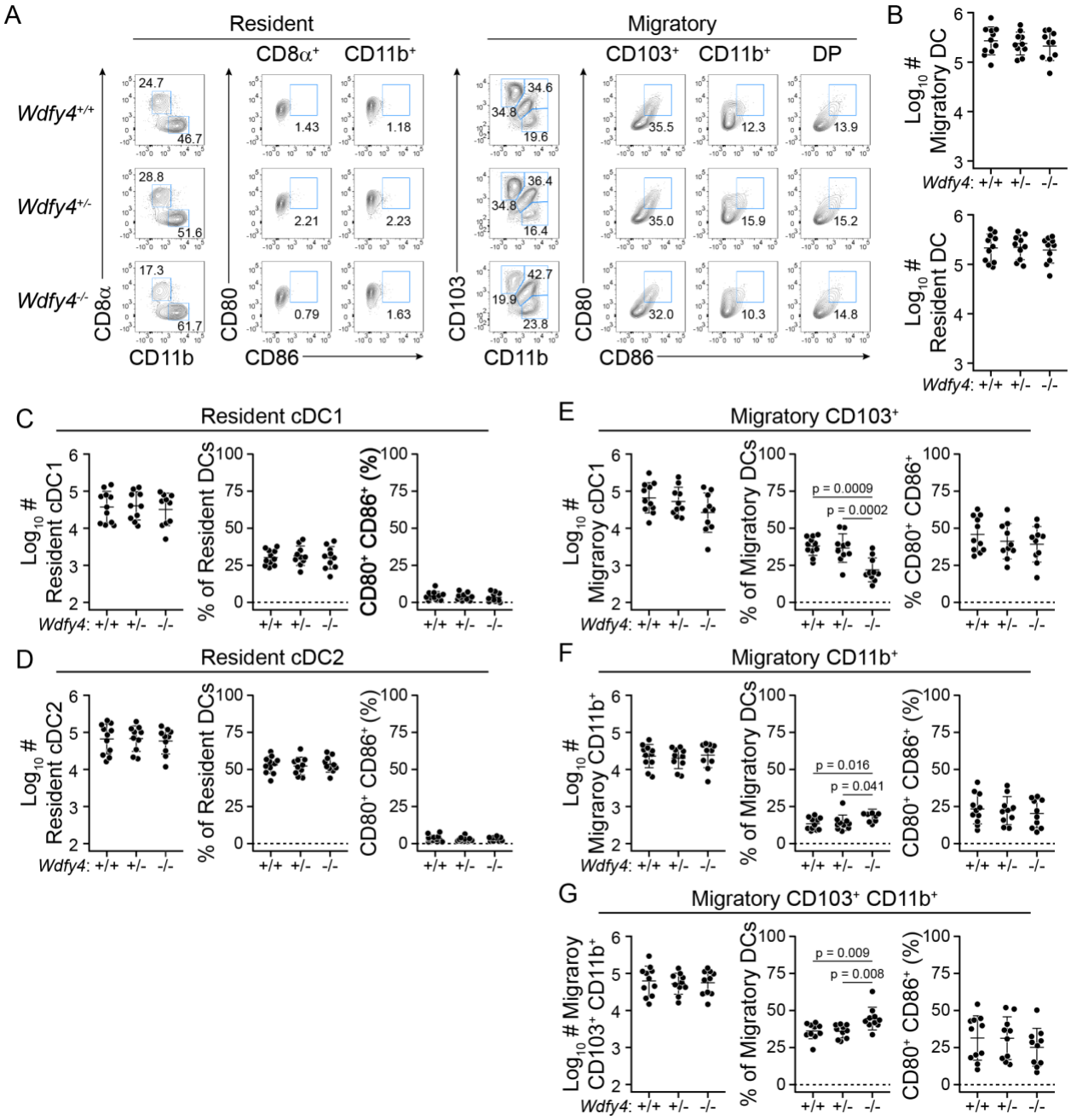

Supplemental Figure S6 (Related to Figure 6): Reduced CD103⁺ cDC1 populations in mesenteric LNs of *Wdfy4*$^{-/-}$ mice. A) Representative flow cytometry plots of cDC populations in pooled mesenteric LNs (mLNs) of *Wdfy4*$^{+/+}$, *Wdfy4*$^{+/-}$, and *Wdfy4*$^{-/-}$ mice. **B)** Resident and migratory cDC numbers in pooled mLNs of *Wdfy4*$^{+/+}$ (n = 11), *Wdfy4*$^{+/-}$ (n = 10), and *Wdfy4*$^{-/-}$ (n = 10) mice. **C-F)** Quantification of number, frequency, and CD80/CD86 expression data for resident

CD8α$^+$ cDC1 (C), resident CD11b$^+$ cDC2 (D), migratory CD103$^+$ cDC1 (E), and migratory CD11b$^+$ cDC2 (F), and migratory CD103$^+$ CD11b$^+$ cDC2 in pooled mLNs (G). Statistical significance was determined by one-way ANOVA with post-hoc Tukey's HSD. Data are pooled from three independent experiments.

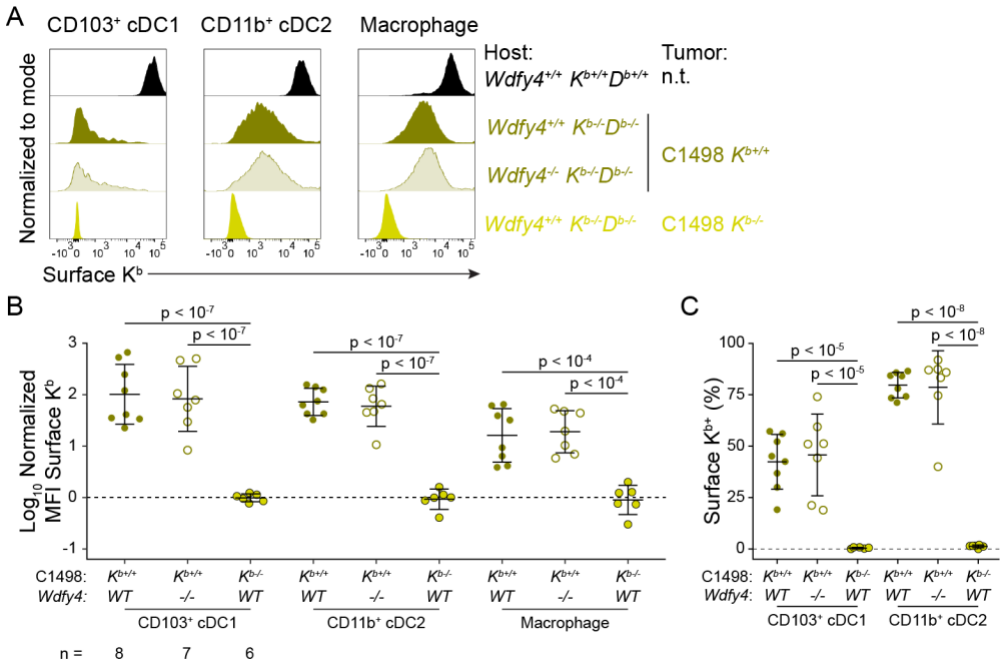

Supplemental Figure S7 (Related to Figure 6): MHC-I cross-dressing occurs independently of WDFY4. *Wdfy4*$^{-/-}$ *K*$^{b-/-}$*D*$^{b-/-}$ and *Wdfy4*$^{+}$ *K*$^{b-/-}$*D*$^{b-/-}$ mice were inoculated with C1498 *K*$^{b+/+}$ or *K*$^{b-/-}$ cells. Tumor-resident APCs were analyzed for acquisition of C1498-derived K^{b} molecules by surface antibody staining and flow cytometry. **A)** Representative flow cytometry histograms. **B)** Summary plot of normalized mean fluorescence intensity. **C)** Summary plot of percent K^{b+} DCs. The *Wdfy4*$^{+}$ group includes four *Wdfy4*$^{+/+}$ and four *Wdfy4*$^{+/-}$ mice. Data are pooled from two independent experiments. Statistical significance was determined by two-way ANOVA with post-hoc Tukey's HSD.